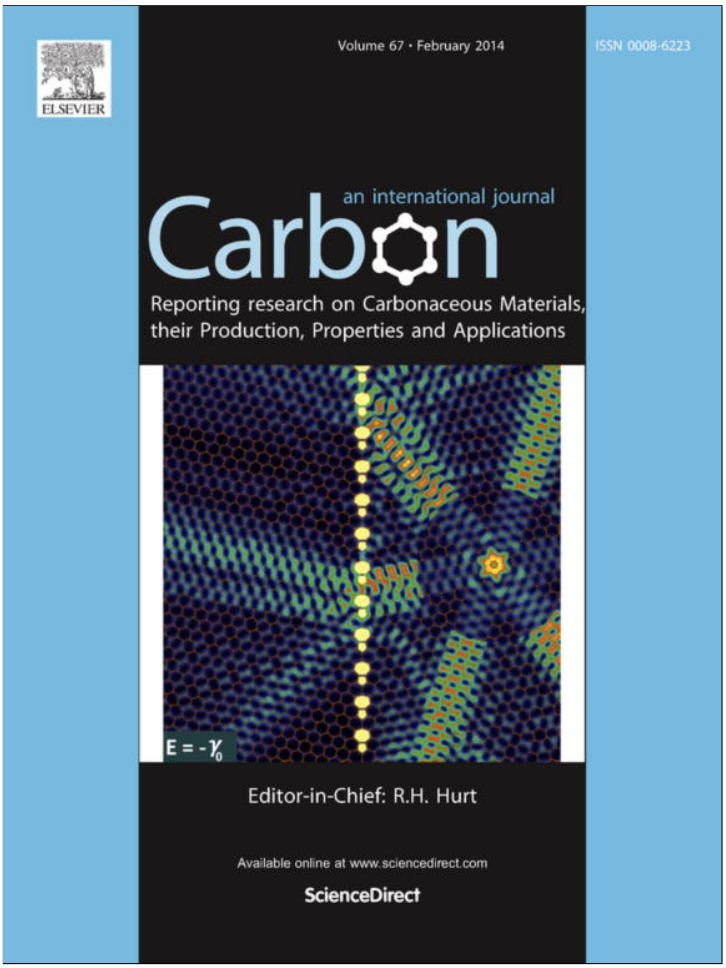

CARBON 67 (2014) 525–533

Available at www.sciencedirect.com

ScienceDirect

journal homepage: www.elsevier.com/locate/carbon

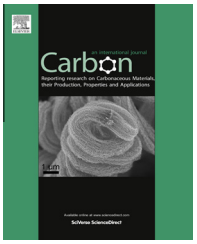

# Catalyst-free, self-assembly, and controllable synthesis of graphene flake–carbon nanotube composites for high-performance field emission

*Jian-Hua Deng* [a,*], *Guo-An Cheng* [b], *Rui-Ting Zheng* [b], *Bin Yu* [a], *Guo-Zheng Li* [a], *Xing-Gang Hou* [a], *Meng-Li Zhao* [a], *De-Jun Li* [a]

[a] *College of Physics and Materials Science, Tianjin Normal University, Tianjin 300387, PR China*

[b] *Key Laboratory of Beam Technology and Material Modification of Ministry of Education, Beijing Normal University, Beijing 100875, PR China*

ARTICLE INFO

*Article history:*
Received 28 September 2013
Accepted 10 October 2013
Available online 18 October 2013

ABSTRACT

Catalyst-free and self-assembled growth of graphene flakes (GFs) on carbon nanotube (CNT) arrays have been realized by using microwave plasma enhanced chemical vapor deposition. The shape of GFs was highly manipulated by adjusting the growth time, C concentration, and microwave power. We qualitatively discussed the nucleation and growth mechanism of GFs based on the growth parameter–GF shape studies. The field emission (FE) properties of graphene flake–carbon nanotube (GF–CNT) composites for different GF shapes were measured and found to be strongly influenced by the GF distribution. The optimal shape of GFs for FE had small scales, sharp edges, and sparse distribution on CNTs. The best FE properties with the optimal shape were observed with a low turn-on electric field of 0.73 V/μm and excellent stability, which are superior to those of the as-grown CNT arrays and GF–CNT composites covered by densely distributed GFs. We consider that the large aspect ratio of CNTs and the unique FE stability of GFs play a synergetic effect on the improved FE properties.



## 1. Introduction

Graphene is a two-dimensional honeycomb C network having fascinating properties [1]. Graphene based materials have aroused intense interest in a wide range of applications such as field effect transistors [2], gas sensors [3], resonators [4], and energy storage [5]. Graphene is also a promising field emission (FE) material due to its atomic thin edges and unique two-dimensional shapes [6–10]. There are many ways to fabricate graphenes, such as mechanical exfoliation [1], chemical exfoliation [11,12], epitaxial growth [13–15], oxidation and thermal expansion [16,17], and thermal chemical vapor deposition (CVD) [18–20]. However, most of these graphenes grow in the form of planar thin films lying down on the substrates, and this morphology has been found to have little FE [21].

To achieve a high-performance FE, the sharp edges of graphenes should be vertical to the substrate, thus the growth of vertically aligned graphenes is important. Previous works on this respect have proven that plasma enhanced chemical vapor deposition (PECVD) is the only way to fabricate vertical graphenes [22–24]. However, except the FE stability, the FE properties of these graphenes are still inferior to those well-verified one-dimensional field emitters such as CNT arrays. It is thus worth expecting that we fabricate composites having advantages of both the graphenes (excellent FE stability) and the CNT arrays (incomparable large aspect ratio). This hybrid material has been obtained and reported in our previous

* *Corresponding author:* Fax: +86 22 23766519.
E-mail address: jhdeng1983@163.com (J.-H. Deng).
0008-6223/$ - see front matter 
http://dx.doi.org/10.1016/j.carbon.2013.10.025

work [25]. In that study, we fabricated few-layer graphene–CNT hybrids by using radio frequency sputtering deposition and studied their FE properties. However, the growth of graphenes in that work was less controllable and the relationship between the graphene shapes and the FE properties of this hybrid material was not discussed, and additionally, the growth mechanism of graphenes was proposed merely based on a conjecture rather than on enough experimental observations. Nevertheless, achieving a controllable growth of vertical graphene on CNTs, deeply understanding its growth mechanism, and finding the optimal shapes for FE are really important, but such attempts so far, to the best of our knowledge, have not been reported.

Herein, we report a strategy to prepare graphene flake–carbon nanotube (GF–CNT) composites by using microwave PECVD. The growth of GFs is catalyst-free and self-assembled. The GF shapes can be highly adjusted by changing growth parameters. The nucleation and growth of GFs is discussed on the basis of a series of comparative experiments. The FE properties of differently shaped GF–CNT composites were tested and found to be strongly dependent on the GF shapes.

## 2. Experimental details

Fig. 1 schematically shows the preparation of GF–CNT composites. The catalyzed growth of CNT arrays by using thermal CVD (step 1 and 2) has been reported previously in detail [25]. The GF growth (step 3) by using microwave PECVD is catalyst-free. In comparison with the radio frequency sputtering deposition we used previously [25], the PECVD here is advantageous for manipulating the GF shapes. Expect the growth time, the C concentration and the plasma power can also be controlled precisely according to our needs, which is helpful for understanding the growth of GFs. $C_2H_2$ and $H_2$ were used as the C feedback and the carrying gas, respectively. The controlled growth of GF–CNT composites were realized by adjusting the growth time, microwave powers, and $C_2H_2/H_2$ ratios.

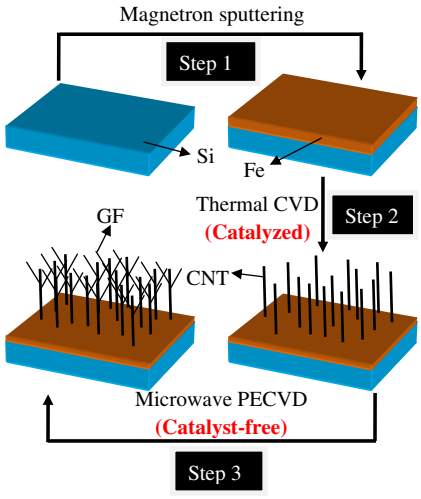


**Fig. 1 – Schematics of the preparation of GF–CNT composites. (A color version of this figure can be viewed online.)**

The morphology and structure of samples were observed by scanning electron microscope (SEM, S-4800, Hitachi, Japan, 10 keV) and transmission electron microscope (TEM, JEM-2010, JEOL, Japan, 200 kV). The crystallinity was analyzed by Raman spectroscopy (LabRAM Aramis, Horiba Jobin Yivon, France) using 633 nm excitation laser. The work function of samples was measured by Photoelectron spectrometer (AC-2, Riken Keiki, Japan, spot area: $4 \times 4$ mm$^2$). The FE tests were carried out by using a diode setup in an ultrahigh vacuum chamber. The details have been described in our previous study [25].

## 3. Results and discussion

### 3.1. GF–CNT composites in different growth stages

Experiments performed in different growth times were carried out to investigate the characteristics of the GF growth stages. In this research, the growth time was set at 10, 20, and 60 min, and the other growth parameters were kept unchanged: 200 W, 1 kPa, 800 °C, $C_2H_2/H_2 = 5/10$ (5 sccm $C_2H_2$ and 10 sccm $H_2$, similarly hereafter). Fig. 2a shows a typical SEM side-view image of as-grown CNTs. The CNTs are about 40–60 nm in diameter, vertically aligned, and well-separated. The SEM images of GF–CNT composites for growth times of 10, 20, and 60 min are shown in Fig. 2b, c, and d, respectively. It can be found that both the density and the size of GFs increase dramatically with the growth times. The GF growth can be roughly inferred by comparing the high-resolution SEM images presented in the insets of Fig. 2a–d. The smooth surface of the as-grown CNT (inset of Fig. 2a) is covered by sparsely distributed nano-particles (inset of Fig. 2b) after the 10-min GF growth, indicating that the GF nucleates in a very short time. And then, the density of these nano-particles increases and the nucleated GFs grow in the form of two-dimensional thin flakes with further increasing the growth times (insets of Fig. 2c and d). The 60 min sample was observed by TEM. Fig. 2e is a TEM image showing randomly distributed GF–CNT composites. The small-scale GFs grow not only on the catalyst encapsulated CNT tips but also on the CNT walls, indicating that the GF growth is catalyst-free. Fig. 2f shows the fine structure of a GF–CNT composite. The orderly arranged C atoms between the GF and the CNT demonstrates that the GF growth is self-assembled. The sharp GF edges, generally less than 10 layers, can facilitate the electron tunneling during FE.

### 3.2. GF–CNT composites synthesized in different C concentrations

Graphene is composed of honeycomb C network, thus the C supply is certain to influence the GF growth greatly. In this research, we barely varied the C concentrations (characterized by $C_2H_2/H_2$ ratios) and kept the other growth parameters unchanged: 100 W, 1 kPa, 800 °C, and 5 h. Fig. 3 shows typical SEM images of GF–CNT composites synthesized in $C_2H_2/H_2$ ratios of (a,b) 1/15, (c,d) 1/10, (e,f) 3/10, and (g,h) 5/10. Outstanding morphological changes are observed. The GFs of sample 1/15 are extremely sparsely distributed and their sizes are less

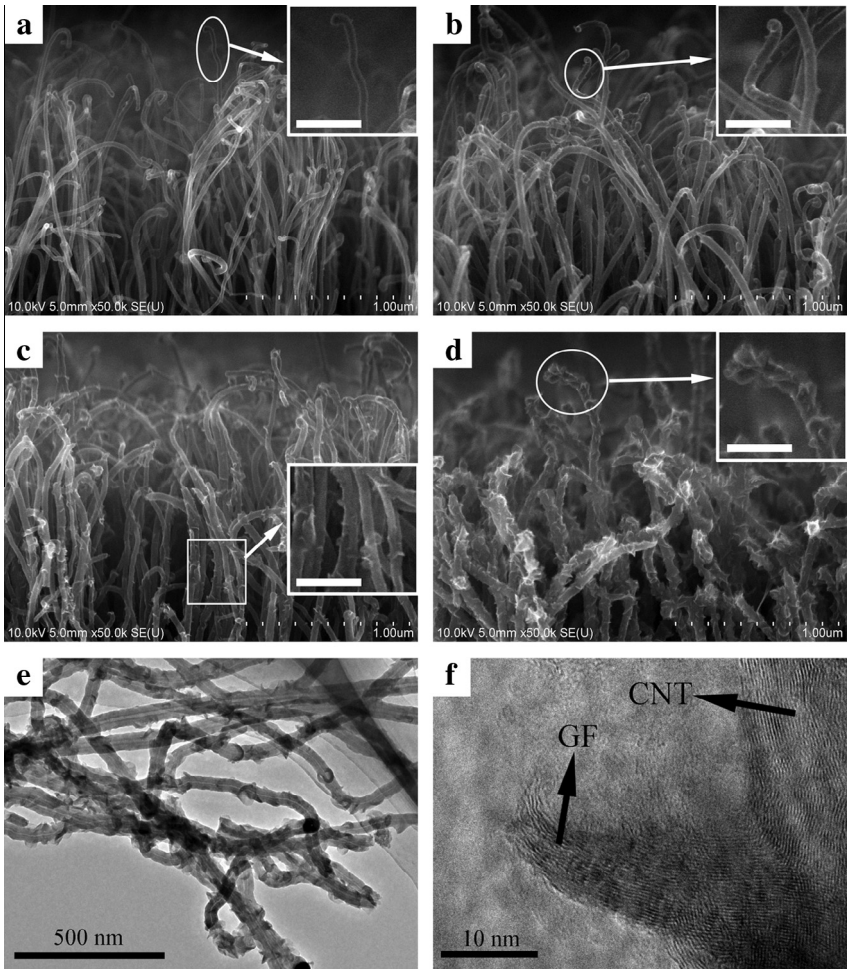


**Fig. 2 – (a) SEM image of as-grown CNTs. (b–d) SEM images of GF–CNT composites for growth times of (b) 10, (c) 20, and (d) 60 min. The insets of (a–d) are the corresponding high-resolution SEM images of the marked parts. Low- (e) and high-resolution (f) TEM images of the 60 min GF–CNT composites. Other growth conditions: 200 W, 1 kPa, 800 °C, $C_2H_2/H_2$ = 5/10 (5 sccm $C_2H_2$ and 10 sccm $H_2$, similarly hereafter). The scale bars in the insets of (a–d) are 200 nm.**

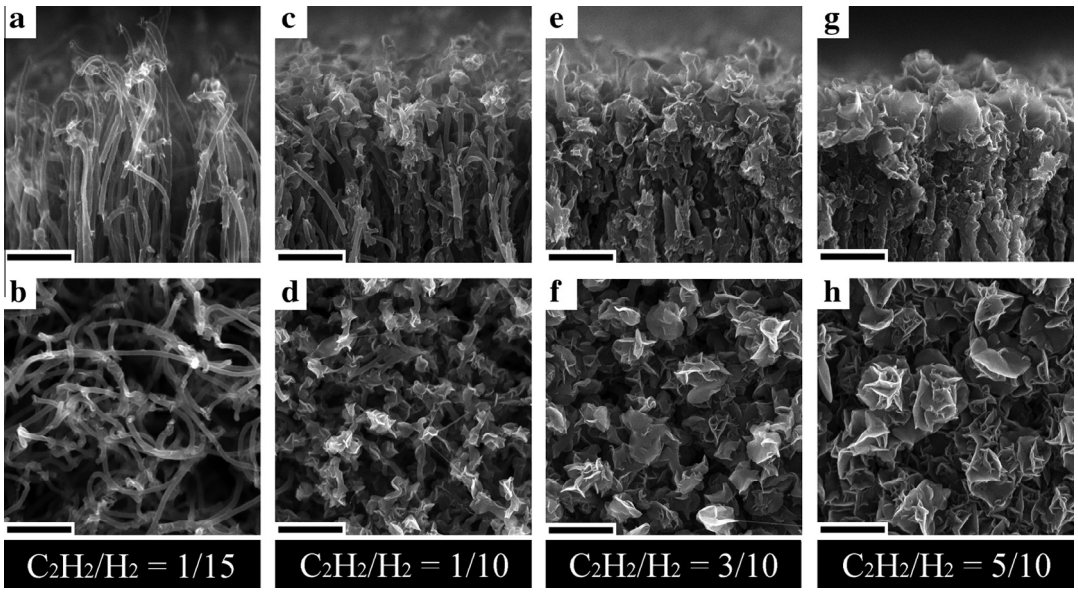


**Fig. 3 – SEM images of GF–CNT composites synthesized in $C_2H_2/H_2$ ratios of (a,b) 1/15, (c,d) 1/10, (e,f) 3/10, and (g,h) 5/10. Other growth conditions: 100 W, 1 kPa, 800 °C, 5 h. All the scale bars are 1 μm.**

than 100 nm (Fig. 3a and b), while for sample 5/10, the GFs are densely distributed on the surface of CNT arrays and their sizes reach 1 μm (Fig. 3g and h), indicating that both the growth rate and the nucleation density of GFs increase with the C concentrations. In addition, the GF distribution along the CNTs also changes with the C supply. It gradually expands from the CNT tips (Fig. 3a) to the deep CNT forests (Fig. 3c) until the interspaces among CNTs are fully filled by amorphous C (Fig. 3e and g).

The fine structure of sample 1/10 and 5/10 was observed by TEM for comparison. The ultrasonicating time for TEM sample preparation is 45 min. Fig. 4a is a typical low-resolution TEM image showing dispersed GF–CNT composites of sample 1/10. It can be seen that each GF–CNT composite is composed of a tubular CNT and several aligned GFs, forming a rose-like appearance. Fig. 4b shows a typical high-resolution TEM image of a 7-layer GF, indicating that our GFs are ultrathin graphenes. The interlayer spacing of the GFs is larger than that of the bulk graphite gap (0.34 nm), suggesting a reduction of the van der Waals interaction. The TEM image of sample 5/10 (Fig. 4c) shows an interesting structural change that barely appears in sample 1/10 and the few-layer graphene samples in our previous study [25]: GFs are broken off from the CNTs. It seems that the connection between GFs and CNTs weakens with increase of C concentrations. We set up a second experiment with decreased ultrasonicating time to identify this question. The inset of Fig. 4c shows a typical TEM image of sample 5/10 prepared using 10-min ultrasonication. It can be seen that the amount of C residuals on the surface of CNTs increases dramatically with the decrease of ultrasonicating time. We attribute this to the influences of C concentrations. In cases of high C concentrations, the quick C atom deposition leaves insufficient time for atom diffusion to form two-dimensional GFs and thus leads to the growth of amorphous C, which makes the subsequent nucleated GFs directly locate on the loosely bonded amorphous C, and those GFs, along with the amorphous C layer, are easy to be broken off during the ultrasonication. However, the thickness of this deposited C layer is negligible or it has been etched away by hydrogen plasma during the nucleation when the C concentration is low, such as in cases of sample 1/10 and the few-layer graphenes fabricated by using radio frequency sputtering deposition [25], resulting in the direct growth of GFs on the CNTs, and these self-assembled GFs are hard be broken off during the ultrasonication. The layers of sample 5/10 are usually more than 15, as shown in Fig. 4d, indicating that the GF thickness also increases with the C concentrations.

Fig. 5 shows Raman spectra (633 nm) of the as-grown CNT arrays, and the GF–CNT composites synthesized in $C_2H_2/H_2$ ratios of 1/15, 1/10, 3/10, and 5/10. For all types of GF

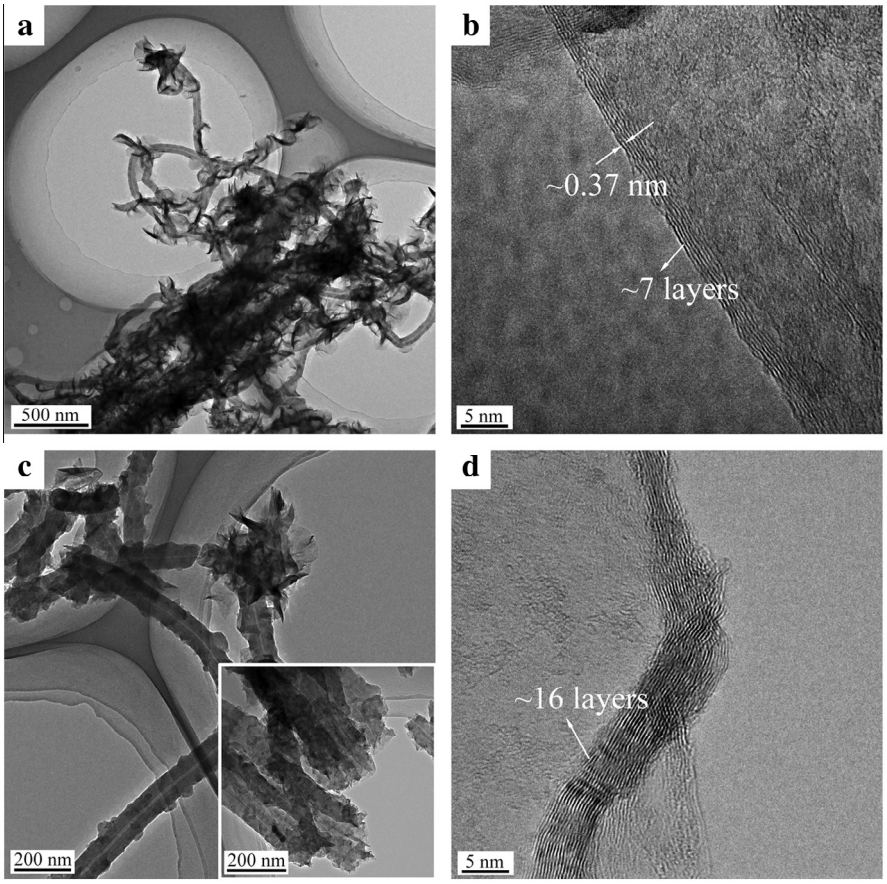


**Fig. 4 – Low- (a and c) and high-resolution (b and d) TEM images of GF–CNT composites synthesized in $C_2H_2/H_2$ ratios of (a,b) 1/10 and (c,d) 5/10. The ultrasonicating time during TEM sample preparation of (a–d) is 45 min. The inset of (c) is a low-resolution TEM image of sample 5/10 prepared using 10-min ultrasonication. Other growth conditions: 100 W, 1 kPa, 800 °C, 5 h.**

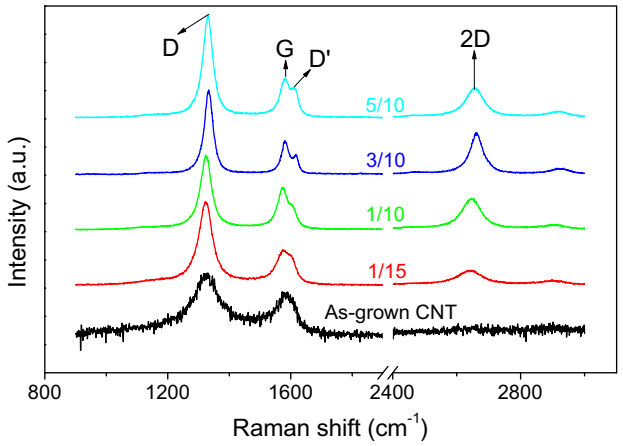


**Fig. 5 – Raman spectra of the as-grown CNT arrays, and the GF–CNT composites synthesized in $C_2H_2/H_2$ ratios of 1/15, 1/10, 3/10, and 5/10. Laser wavelength: 633 nm. (A color version of this figure can be viewed online.)**

composites, a symmetric single 2D peak at around 2647 $cm^{-1}$ is observed. The intensity ratio of 2D peak to the graphite related G peak ($I_{2D}/I_G$) is usually used to distinguish single-, bi-, and multi-layer graphenes [26–28]. It is important to note that the $I_G$ only contains Raman contribution from graphenes, which means that this evaluation is inappropriate in our GF–CNT system. However, we can roughly use the $I_{2D}/I_G$ ratio to evaluate the GFs of sample 3/10 and 5/10, the CNTs of which are almost covered by GFs (Fig. 3f and h). The sample 3/10 has the largest $I_{2D}/I_G$ ratio: 1.24, indicating that our GFs are ultrathin graphenes [26]. The $I_{2D}/I_G$ ratio decreases when the $C_2H_2/H_2$ ratio increases from 3/10 to 5/10, demonstrating that the thickness of GFs increases with the C concentrations, in good agreement with our previous TEM observations. The disordered C related D peak around 1332 $cm^{-1}$ indicates that our GFs are defective [26].

### 3.3. *The influences of microwave power on the growth of GF–CNT composites*

Fig. 6a, b, and c show SEM side-view images of GF–CNT composites synthesized at 400, 600, and 800 W, respectively. For the other growth parameters, we chose the same as those used in the fabrication of sample 5/10 above mentioned: $C_2H_2/H_2$ = 5/10, 1 kPa, 800 °C, and 5 h. By comparison, it can be seen that both the density and the size of GFs together with the amount of amorphous C on the surface of CNTs decrease with the increase of microwave power from 100 to 400 W. We further promoted the microwave powers and found that no GF was obtained at 600 W (Fig. 6b) and even the CNT arrays disappeared at 800 W (Fig. 6c). We consider that the microwave power related hydrogen plasma etching on C is responsible for these morphological changes.

### 3.4. *Discussions on the growth of GFs*

We have proposed a nucleation and growth mechanism of few-layer graphenes in our previous study but only on the ba-

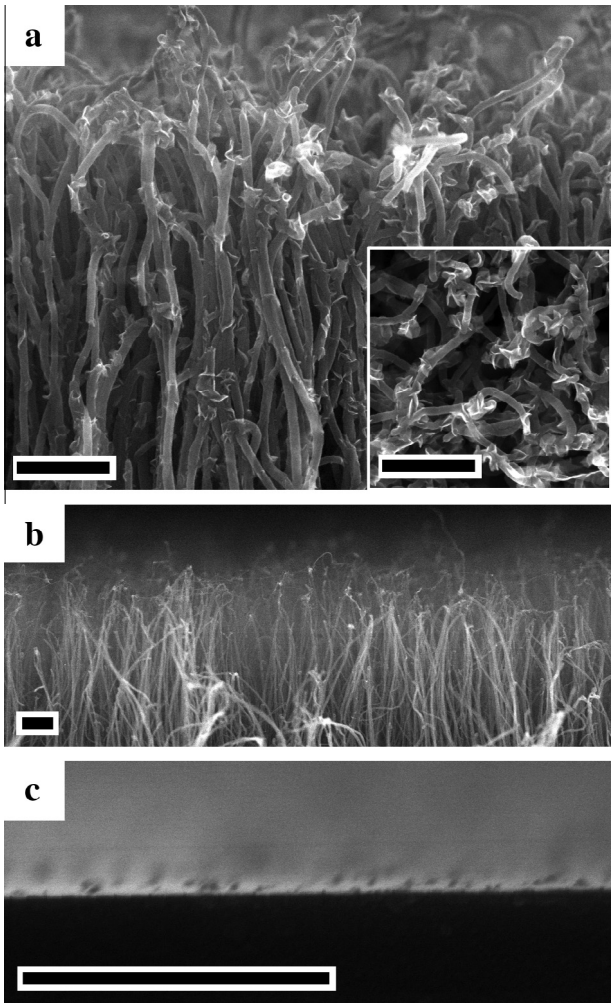


**Fig. 6 – SEM side-view images of GF–CNT composites synthesized at (a) 400, (b) 600, and (c) 800 W, the inset of (a) is a corresponding SEM top-view image. Other growth conditions: $C_2H_2/H_2$ = 5/10, 1 kPa, 800 °C, and 5 h. All the scale bars are 500 nm.**

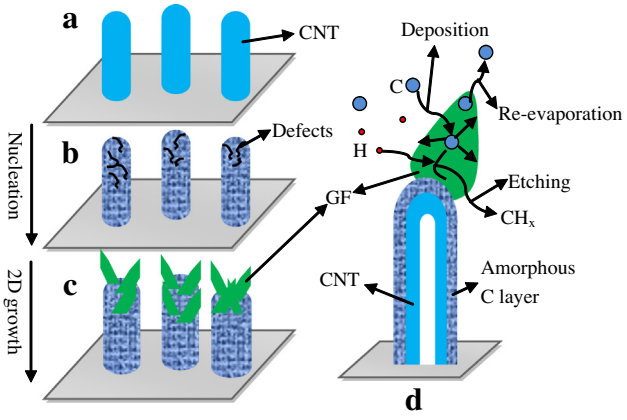


**Fig. 7 – (a–c) Schematics of the nucleation (a → b) and the two-dimensional (2D) growth (b → c) of GFs. (d) Schematic illustration of the growth of GFs. (A color version of this figure can be viewed online.)**

sis of a conjecture for lack of enough experimental observations [25]. In the present research, this growth mechanism will be further discussed based on the above growth parameter–GF shape researches. Fig. 7a–c schematically shows the nucleation (a → b) and the two-dimensional growth (b → c) of GFs. The catalyst-free growth of GFs follows the vapor–solid mechanism [25], which is different from the catalyzed CVD graphenes that follows the vapor–liquid–solid mechanism [18–20]. Deposited C atoms diffuse on the surface of CNTs and aggregate by means of forming covalent bonds at intrinsic defects of CNTs, resulting in the nucleation of GFs (Fig. 7a → b). The two-dimensional growth of GFs (Fig. 7b → c) has been studied in previous studies [29–31]. Their discussions are proposed on the basis of an assumption that one C atom diffuses on the surface of a flawless graphene, and the surface diffusion length of this C atom before re-evaporation [29] is:

$$\lambda_d = 2a_0 \exp\left(\frac{E_a - E_d}{2\kappa T}\right) \quad (1)$$

where $E_a$ (1.8 eV) is the surface absorbing energy [30], and $E_d$ (0.13 eV) is the surface diffusion energy [31]. In our growth conditions ($a_0$ = 0.14 nm, $T$ = 1073 K, and $\kappa = 1.381 \times 10^{-23}$ J K$^{-1}$), the $\lambda_d$ is 2.3 μm, far larger than the actual sizes of our GFs (less than 1 μm in most cases). We attribute this to that the actual GF growth conditions are quite different from that they assumed in their discussions. First, atom–atom collision during C atom diffusion is inevitable in actual GF growth conditions, making C atoms migrate along curved rather than straight lines, which greatly decreases the actual linear distance ($\lambda_{a,d}$, a C atom can diffuse along the surface of GF before re-evaporation). It should be mentioned that the C concentrations in this study are much higher than that in the fabrication of few-layer graphenes [25], thus the atom–atom collision is much fierce here. Second, diffusing C atoms may be captured by defects that already exist on the surface of GFs, resulting in the decrease of $\lambda_{a,d}$ and the thickening of GFs, for example, the GFs of sample 5/10 are thicker than the sample 1/10 (Fig. 4). This may, in cases of high C concentrations such as sample 5/10, lead to the growth of small-scale GFs on the surface of larger ones forming a flower-like appearance, as shown in Fig. 3h.

Based on the above growth parameter–GF shape discussions, we propose here a qualitative analysis of the growth of GFs, as schematically shown in Fig. 7d. In our research, the growth rate of GFs ($v_{GF}$) is determined by the C atom deposition rate ($v_C$, mainly controlled by the C concentration, Cc), the re-evaporation rate ($v_{r-e}$, mainly controlled by the temperature, $T$), and the hydrogen plasma etching rate ($v_H$, mainly controlled by the microwave power, $P$). Thus the $v_{GF}$ can be expressed as the following function:

$$v_{GF} = f(v_C(C_c) - v_{r-e}(T) - v_H(P)) \quad (2)$$

Since $T$ was kept unchanged in this study, the growth of GFs is merely influenced by the $C_C$ and the $P$. GF grows when $v_C$ is predominant and/or $v_H$ is negligible, corresponding to our GFs synthesized at 100 W (Fig. 3). Concomitantly, the relatively weak hydrogen plasma etching leads to the deposition of amorphous C and thus the thickening of CNTs especially when the C supply is sufficiently enough (Fig. 3e and g). GF grows slowly or no GF grows when $v_H$ is predominant, corresponding to our GFs shown in Fig. 6. In this condition, a great many C atoms leave the surface of GFs by means of forming gaseous $CH_x$, leading to the decrease of the actual C supply on the surface of GFs and thus the decrease of $v_{GF}$.

### 3.5. *FE properties of GF–CNT composites*

FE properties of four types of GF–CNT composites (sample 1/10, 3/10, 5/10, and 400 W), together with as-grown CNT arrays, were tested. Prior to the FE tests, an aging process was taken at ~10 mA/cm$^2$ for 5 h to weaken influences such as absorbates induced promotion [32] and Joule heating induced degradation on FE properties [10]. Fig. 8a shows the plots of $J$ (emission current density) as a function of $E$ (applied field), and the corresponding FE results are shown in Table 1. In comparison with the as-grown CNT arrays, the sample 1/10 and the sample 400 W, both of which are covered by sparsely distributed GFs, show evident FE improvements. Sample 1/10 has excellent FE properties. Its turn-on ($E_{on}$, 0.73 V/μm at 10 μA/cm$^2$) and threshold field ($E_{th}$, 1.16 V/μm at 10 mA/cm$^2$) are much lower than those of the other four types of samples and plenty of well-verified field emitters such as single-layer graphene films [6], single-crystalline boron nanowire arrays [33], and single-crystalline $Sb_2Se_3$ nanowires [34]. The poor FE properties of sample 3/10 and 5/10, which are covered by densely distributed GFs, indicate that the FE of GF–CNT composites is dependent on the GF coverage. Replotting of the data as $\ln(J/E^2)$ versus $1/E$, as shown in the inset of Fig. 8a, indicates typical $F$–$N$-type FE behavior [35]. The work function ($\Phi$) of the GF–CNT composites, varying from 4.67–4.75 eV, is smaller than that of the as-grown CNT arrays (4.89 eV). This decrease of work function is attributed to the ascended Fermi level induced by the increased state density of defects after the longtime plasma processing [36]. The field enhancement factor ($\beta$), which is a geometric parameter closely related to the shape of emitters, is determined by the work function and the constant $F$–$N$ slope at the low-current region [35], as shown in Table 1. Sample 1/10, which has the best FE properties among the five, has the largest $\beta$ (~6244), indicating that the FE properties of GF–CNT composites are mainly determined by their geometric morphology. The FE properties of sample 3/10 and 5/10 are much closer to those of graphene arrays grown on planar substrates [25]. This is mainly due to that the fully filled amorphous C of these two samples makes the CNT arrays more like planar substrates and thus shield the field enhancement from CNTs. This means that the CNTs play a significant role in improving the FE properties of GF–CNT composites. In comparison with few-layer graphenes we fabricated previously [25], the sample 1/10 has far better FE properties, indicating that obtaining optimal shapes is very important for fabricating high-performance field emitters.

The FE stability at ~10 mA/cm$^2$ of the as-grown CNT arrays and GF–CNT composites having the best (sample 1/10) and the worst (sample 5/10) FE properties were monitored, as shown in Fig. 8b. $J_{drop}$ ($J$ degradation in 10 h) is used to evaluate the stability. It is calculated by $(J_{first}-J_{last})/J_m$, where the $J_{first}$, $J_{last}$, and $J_m$ are the first, the last, and the mean emission current densities during stability tests, respectively. In comparison with the remarkable $J_{drop}$ of the as-grown CNT arrays

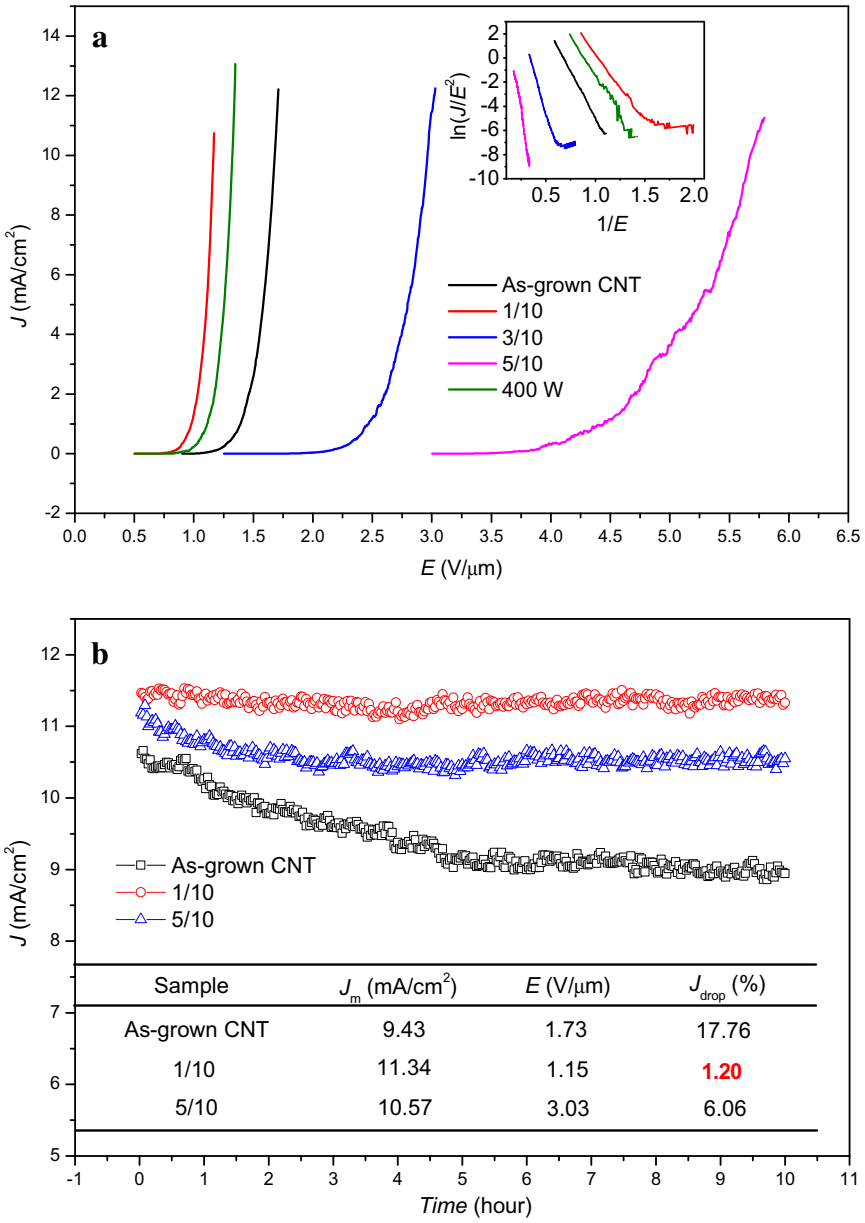


**Fig. 8 – FE properties of as-grown CNT arrays and GF–CNT composites synthesized at $C_2H_2/H_2$ ratios of 1/10, 3/10, 5/10, and 400 W. (a) *J–E* curves, and the inset is the corresponding *F–N* plots. (b) FE stability of the as-grown CNT arrays, the sample 1/10, and the sample 5/10, presented in terms of *J* versus *Time*. *E*: applied field, $J_m$: mean emission current density, $J_{drop}$: emission current density degradation. (A color version of this figure can be viewed online.)**

**Table 1 – Turn-on ($E_{on}$), threshold field ($E_{th}$), work function ($\Phi$) and field enhancement factor ($\beta$) of the as-grown CNT arrays, sample 1/10, 3/10, 5/10, and 400 W.**

| Sample | $E_{on}$ (V/μm) | $E_{th}$ (V/μm) | $\Phi$ (eV) | $\beta$ |
|---|---|---|---|---|
| As-grown CNT | 1.02 | 1.68 | 4.89 | 4799 |
| 1/10 | 0.73 | 1.16 | 4.69 | 6244 |
| 3/10 | 1.83 | 2.96 | 4.74 | 2447 |
| 5/10 | 3.37 | 5.67 | 4.67 | 1416 |
| 400 W | 0.82 | 1.32 | 4.75 | 5677 |

(17.76%), the $J_{drop}$ of the GF–CNT composites is far smaller (1.20% for sample 1/10 and 6.06% for sample 5/10), in good agreement with our anticipation. This improved FE stability is mainly due to the weakening of Joule heating induced emitting site burning by taking use of the unique two-dimensional structure of GFs [10]. Furthermore, the low applied field of

sample 1/10 (1.15 V/μm), much lower than that of the other four types of samples, is favorable in practical applications.

## 4. Summary

We have demonstrated a catalyst-free, self-assembled, and vapor–solid approach to synthesize GFs on CNT arrays by using microwave PECVD. The GF shapes can be highly controlled by adjusting the growth time, C concentration, and microwave power. The nucleation and growth mechanism of GFs is discussed and qualitative analyses are given based on a series of comparative experiments. Comparison of the FE properties of differently shaped GF–CNT composites indicate that the FE performance is strongly influenced by the GF distribution on CNTs. GFs with small scales, sharp edges, and sparse distribution on CNTs are suitable for high-performance FE. GF–CNT composites with densely covered GFs have poor FE properties due to the shield of field enhancement from CNTs. The growth of GFs on CNTs can greatly improve their FE stability. Our results indicate that GF–CNT composite is a promising material in developing high-performance FE devices. Furthermore, this self-assembled and controllable growth of GFs may also find applications in some other fields such as fabricating high-performance supercapacitors based on GF-three-dimensional graphene network composites, and works on this aspect are being done and will be published in the future.

## Acknowledgments

This work was supported by the National Natural Science Foundation of China for Youth Science Funds (Nos. 51302187, 51302188, and 11204215), the National Basic Research Program of China (2010CB832905), the National Natural Science Foundation of China (51272176), the Tianjin High School Science & Technology Foundation (20120312), the Tianjin Natural Science Foundation (Nos. 13JCZDJC33900 and 12JCYBJC32500), and the Natural Science Foundation (5RL119), the Application Development Foundation (52XK1207), and the Youth Foundation (52XQ1204) of Tianjin Normal University.

## REFERENCES

[1] Novoselov KS, Geim AK, Morozov SV, Jiang D, Zhang Y, Dubonos SV, et al. Electric field effect in atomically thin carbon films. Science 2004;306(5696):666–9.
[2] Lin YM, Dimitrakopoulos C, Jenkins KA, Farmer DB, Chiu HY, Grill A, et al. 100-GHz transistors from wafer-scale epitaxial graphene. Science 2010;327(5966):662.
[3] Schedin F, Geim AK, Morozov SV, Hill EW, Blake P, Katsnelson MI, et al. Detection of individual gas molecules adsorbed on graphene. Nat Mater 2007;6:652–5.
[4] Bunch JS, van der Zande AM, Verbridge SS, Frank IW, Tanenbaum DM, Parpia JM, et al. Electromechanical resonators from graphene sheets. Science 2007;315(5811):490–3.
[5] Zhou M, Lin TQ, Huang FQ, Zhong YJ, Wang Z, Tang YF, et al. Highly conductive porous graphene/ceramic composites for heat transfer and thermal energy storage. Adv Funct Mater 2013;23(18):2263–9.
[6] Wu ZS, Pei SF, Ren WC, Tang DM, Gao LB, Liu BL, et al. Field emission of single-layer graphene films prepared by electrophoretic deposition. Adv Mater 2009;21(17):1756–60.
[7] Qian M, Feng T, Ding H, Lin LF, Li HB, Chen YW, et al. Electron field emission from screen-printed graphene films. Nanotechnology 2009;20(42):425702 (6pp).
[8] Lahiri I, Verma VP, Choi W. An all-graphene based transparent and flexible field emission device. Carbon 2011;49(5):1614–9.
[9] Huang CK, Ou YX, Bie YQ, Zhao Q, Yu DP. Well-aligned graphene arrays for field emission displays. Appl Phys Lett 2011;98(26):263104 (3pp).
[10] Dean KA, Burgin TP, Chalamala BR. Evaporation of carbon nanotubes during electron field emission. Appl Phys Lett 2001;79(12):1873–5.
[11] Dimiev A, Kosynkin DV, Sinitskii A, Slesarev A, Sun ZZ, Tour JM. Layer-by-layer removal of graphene for device patterning. Science 2011;331(6021):1168–72.
[12] Gilje S, Han S, Wang MS, Wang KL, Kaner RB. A chemical route to graphene for device applications. Nano Lett 2007;7(11):3394–8.
[13] Berger C, Song ZM, Li XB, Wu XS, Brown N, Naud C, et al. Electronic confinement and coherence in patterned epitaxial graphene. Science 2006;312(5777):1191–6.
[14] Berger C, Song ZM, Li TB, Li XB, Ogbazghi AY, Feng R, et al. Ultrathin epitaxial graphite: 2D electron gas properties and a route toward graphene-based nanoelectronics. J Phys Chem B 2004;108(52):19912–6.
[15] Yakes MK, Gunlycke D, Tedesco JL, Campbell PM, Myers-Ward RL, Eddy Jr CR. Conductance anisotropy in epitaxial graphene sheets generated by substrate interactions. Nano Lett 2010;10(5):1559–62.
[16] McAllister MJ, Li JL, Adamson DH, Schniepp HC, Abdala AA, Liu J, et al. Single sheet functionalized graphene by oxidation and thermal expansion of graphite. Chem Mater 2007;19(18):4396–404.
[17] Wei ZQ, Barlow DE, Sheehan PE. The assembly of single-layer graphene oxide and graphene using molecular templates. Nano Lett 2008;8(10):3141–5.
[18] Bao QL, Zhang H, Wang Y, Ni ZH, Yan YL, Shen ZX, et al. Atomic-layer graphene as a saturable absorber for ultrafast pulsed lasers. Adv Funct Mater 2009;19(19):3077–83.
[19] Avsar A, Yang TY, Bae S, Balakrishnan J, Volmer F, Jaiswal M, et al. Towards wafer scale fabrication of graphene based spin valve devices. Nano Lett 2011;11(6):2363–8.
[20] Kim KS, Zhao Y, Jang H, Lee SY, Kim JM, Kim KS, et al. Large-scale pattern growth of graphene films for stretchable transparent electrodes. Nature 2009;457:706–10.
[21] Xiao ZM, She JC, Deng SZ, Tang ZK, Li ZB, Lu JM, et al. Field electron emission characteristics and physical mechanism of individual single-layer graphene. ACS Nano 2010;4(11):6332–6.
[22] Wu YH, Yang BJ. Effects of localized electric field on the growth of carbon nanowalls. Nano Lett 2002;2(4):355–9.
[23] Zhu MY, Wang JJ, Holloway BC, Outlaw RA, Zhao X, Hou K, et al. A mechanism for carbon nanosheet formation. Carbon 2007;45(11):2229–34.
[24] Zhang Y, Du JL, Tang S, Liu P, Deng SZ, Chen J, et al. Optimize the field emission character of a vertical few-layer graphene sheet by manipulating the morphology. Nanotechnology 2012;23(1):015202 (6pp).
[25] Deng JH, Zheng RT, Zhao Y, Cheng GA. Vapor-solid growth of few-layer graphene using radio frequency sputtering deposition and its application on field emission. ACS Nano 2012;6(5):3727–33.

[26] Ferrari AC, Meyer JC, Scardaci V, Casiraghi C, Lazzeri M, Mauri F, et al. Raman spectrum of graphene and graphene layers. Phys Rev Lett 2006;97(18):187401 (4pp).
[27] Tuinstra F, Koenig JL. Raman spectrum of graphite. J Chem Phys 1970;53(3):1126–30.
[28] Nemanich RJ, Solin SA. First- and second-order Raman scattering from finite-size crystals of graphite. Phys Rev B 1979;20(2):392–401.
[29] Lewis B, Anderson JC. Nucleation and growth of thin films. London: Academic Press Inc.; 1979. p. 51.
[30] Louchev OA, Sato Y, Kanda H. Growth mechanism of carbon nanotube forests by chemical vapor deposition. Appl Phys Lett 2002;80(15):2752–4.
[31] Lee YH, Kim SG, Tománek D. Catalytic growth of single wall carbon nanotubes. Phys Rev Lett 1997;78(12):2393–6.
[32] Maiti A, Andzelm J, Tanpipat N, von Allmen P. Effect of adsorbates on field emission from carbon nanotubes. Phys Rev Lett 2001;87(15):155502 (4pp).
[33] Liu F, Tian JF, Bao LH, Yang TZ, Shen CM, Lai XY, et al. Fabrication of vertically aligned single crystalline boron nanowire arrays and investigation on their field emission behaviors. Adv Mater 2008;20(13):2609–11.
[34] Zhai TY, Ye MF, Li L, Fang XS, Liao MY, Li YF, et al. Single-crystalline $Sb_2Se_3$ nanowires for high-performance field emitters and photodetectors. Adv Mater 2010;22(40):4530–3.
[35] Fowler RH, Nordheim L. Electron emission in intense electric fields. Proc R Soc London A 1928;119(781):173–81.
[36] Kim G, Jeong BW, Ihm J. Deep levels in the band gap of the carbon nanotube with vacancy-related defects. Appl Phys Lett 2006;88(19):193107 (3pp).